

Date of publication xxxx 00, 0000, date of current version xxxx 00, 0000.

Digital Object Identifier 10.1109/ACCESS.2024.0429000

Scanning Sonar Data from an Underwater Robot with Ground Truth Localization

TIM HANSEN¹, BOGDAN BELENIS¹, MIGUEL BANDE FIRVIDA², TOM CREUTZ², and ANDREAS BIRK¹

¹Constructor University Bremen, School of Computer Science and Engineering, Bremen, 28759, Germany

²Deutsches Forschungszentrum für Künstliche Intelligenz (DFKI), Robotics Innovation Center, Bremen, 28359, Germany

Corresponding author: Andreas Birk (e-mail: abirk@constructor.university).

This work was supported in part by the Deutsche Forschung Gemeinschaft (DFG) in the project "Unconstrained Synthetic Aperture Sonar (U-SAS)" and by the Federal Ministry for Economic Affairs and Climate Action (BMWK) in the project "TRIPLE-GNC".

ABSTRACT Mechanical Scanning Sonars (MSS) are popular underwater sensors for Unmanned Underwater Vehicles (UUV) due to their low cost, small size, and low power consumption. But due to their simplicity, there are also many research challenges related to their usage. Unfortunately, there is also a lack of data with ground truth UUV localization. We provide MSS datasets using a UUV with standard navigation sensors, i.e., an Inertial Measurement Unit (IMU) and a Doppler Velocity Log (DVL). The UUV is globally localized with a high precision optical tracking system in a large research pool to provide ground truth. The data is of interest for multiple research areas related to MSS, e.g., extraction of range information, registration of sonar scans, and especially mapping including Simultaneous Localization and Mapping (SLAM). Different parameter settings and environment conditions are covered, e.g., dynamics in the scene. The IMU and DVL data is also of interest for research on navigation independent of the MSS data. Results from navigation and mapping with an Extended Kalman Filter (EKF) are in addition provided as baseline solutions.

INDEX TERMS marine robotics, mechanical scanning sonar, mechanical scanning imaging sonar, navigation, simultaneous localization and mapping (SLAM), optical tracking, ground truth data

I. INTRODUCTION

SONAR is an essential sensor for underwater machine perception in general and marine robotics in particular. There exist several device classes, which substantially differ in their design and operation principles, physical parameters like size and power consumption, cost, and intended application scenarios. And while sonar is a well established technology, there is also still a substantial amount of research related to it - ranging from the fundamental principles of device design and signal processing up to the way the sensors are used. But in particular for mapping with sonar and the related required methods like navigation, registration, and Simultaneous Localization and Mapping (SLAM), there is a lack of datasets suited for a proper quantitative analysis. This holds especially with respect to widely used low-cost devices in form of mechanical scanning sonars (MSS).

There is an abundance of sonar data related to bathymetry, e.g., provided by the National Oceanic and Atmospheric Administration (NOAA) [1]. These datasets have a very high relevance for, e.g., marine science, but they are not well suited to study mapping and the related methods of underwater machine perception in the context of marine robotics.

First and foremost, there is no ground truth information of the environment for these datasets. In contrary, the sea-floor topology of interest is actually generated from the sonar data. Second, the data is recorded with surface vessels that have access to Global Navigation Satellite Systems (GNSS). At first glance, this is an advantage as this data could be used as a kind of ground truth for localization. But it also implies that core navigation sensors for marine robotics like a Doppler Velocity Log (DVL) are not required. And even if data from (some) navigation sensors was fused into the generation of the bathymetry, it is not included in the datasets as only the resulting maps with GNSS data for georeferencing are of interest. Third, the bathymetry in these datasets tends to cover large-scale areas up to whole oceans, which go way beyond marine robotics use-cases like obstacle avoidance or mapping of man-made structures like marinas or harbors, where in contrast more fine-grain resolutions are required.

In addition to bathymetry data, typically generated with multibeam echosounders (MBES), there is also a strong interest in sonar images from side-scan sonar (SSS) or acoustic cameras that are also sometimes known as forward looking

sonars (FLS). Typical use-cases are object detection and localization, e.g., [2]–[8]. Related data-sets contain sonar-data plus hand-labeled classifications of objects or environment types as ground truth. They inherently neither require nor provide ground truth navigation data.

Within research on mapping with MSS and related methods, e.g., [9]–[23], the state-of-the-art is rife with qualitative evaluations of the results, especially in form of visualizations of generated maps. For a quantitative analysis, the Abandoned Marina dataset recorded in St. Pere Pescador, Spain [22] is a popular choice. The dataset consists of recordings from a Tritech Miniking MSS, a SonTek Argonaut DVL, and a digital compass. The robot, an Ictineu Autonomous Underwater Vehicle (AUV), is operated close to the surface. Hence, access to the Global Positioning System (GPS) via a buoy is feasible and it is recorded as ground truth reference for localization. As ground truth reference of the environment, a satellite image is provided.

While the Abandoned Marina dataset is useful for quantitative evaluations, it also has its severe drawbacks. First, GPS data only provides position information and there is no ground truth for orientation. The digital compass at best provides some rough references and its data is needed for fusion with the DVL, i.e., it is part of the solution that is to be evaluated. There is hence no full pose information for the localization reference. Second, the accuracy of the GPS corresponds to the state-of-the-art of 2006 when the data was recorded, i.e., it is far from the 1 – 2cm accuracy of, e.g., Real Time Kinematic (RTK) GPS used nowadays. Third, the dataset is based on a single trajectory of the vehicle with static parameter settings.

We aim to overcome these limitations with our Bremen MSS Datasets. First of all, we use an optical tracking system, which provides both position and orientation information, i.e., the full pose as ground truth localization. Second, there is a much higher accuracy of the ground truth. Third, data is recorded in multiple trials with different device parameter settings. Fourth, variations of environment conditions are included, e.g., by running two MSS in parallel leading to a relevant, non-trivial increase in the noise level, as well as by using a 2nd robot to generate dynamics in the scene.

II. SENSORS, VEHICLE, AND METHODS FOR DATA-ACQUISITION

A. MECHANICAL SCANNING SONARS

A mechanical scanning sonar (MSS), also known as scanning sonar (SS) or mechanical scanning imaging sonar (MSIS), is one of the most simple types of sonar. It features a single beam that is mechanically rotated. Along the beam, or more precisely, along the time axis, the amplitudes of the returns are provided, i.e., the intensity of each return of an emitted ping ordered by time-of-flight. This allows the rendering of a polar image, also known as scan, by stepping through a sequence of angles. MSS have the advantage that they are low cost and they are easy to integrate due to their small size and low power-consumption. Two different popular MSS are

used in the trials for the Bremen data, namely a BlueRobotics Ping360 and a Tritech Micron DST Sonar.

The BlueRobotics Ping360 is a low-cost MSS, if not the most affordable device of this type on the market. It emerged in recent years in the context of open-source components for marine robotics and it is positioned as an add-on for the BlueRobotics BlueROV2, which is also used as vehicle in our trials (Fig.1). Due to the open interfaces of the Ping360, it can also be easily integrated on other vehicles. The Tritech Micron Sonar is a well-established product that is available for more than a decade. It is hence widely used in academia and industry. It uses a chirped pulse to increase the signal robustness and it has among others a higher depth rating than the Ping360 - there even exists a deep-sea ready version suited for operations down to 3,000m depth. The core mechanical and electrical parameters of both products are summarized in Table 1. The basic sensor parameters for both MSS are provided in Table 2.

The two sensors are mounted on the vehicle in two different modes, namely forward-looking for the Ping360 and down-looking or bathymetry mode for the Micron DST. This allows among others a recording of both sensors in parallel, which allows the investigation of topics like the influence of cross-talk on sensor data quality as discussed later on.

B. THE VEHICLE AND THE NAVIGATION SENSORS

The vehicle used for the data collection is a BlueRobotics BlueROV2 in the heavy configuration with a payload skid [24] (Fig.1). It is used as Remotely Operated Vehicle (ROV) in the trials, i.e., it is connected with a tether to a control station in form of a laptop.

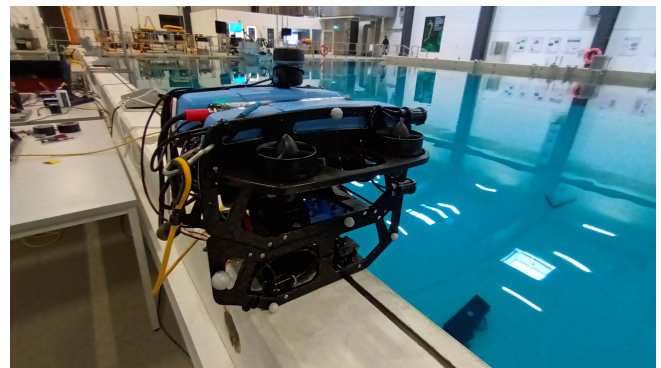


FIGURE 1: A picture of the BlueROV2 vehicle used for the recording of the data.

Due to the slow speed of sound compared to, e.g., RF-signals, the time to take a scan is in the range of multiple (tens of) seconds depending on factors like the maximum range, i.e., the power of the ping, the stepping angle of the MSS, and its field of view. As a consequence, there is the need for motion-compensation when the sensor is mounted on a moving platform like an Unmanned Underwater Vehicle (UUV) even just to generate a single scan.

| | dimensions | weight | | (center) frequ. | (aver.) power | depth rat. |
|------------|----------------------------|-------------|---------------|-----------------|---------------|------------|
| | $H \times L \times W$ [mm] | in air [gr] | in water [gr] | [kHz] | [W] | [m] |
| Ping360 | $83 \times 89 \times 77$ | 510 | 175 | 750 | 5 | 300 |
| Micron DST | $79 \times 56 \times 50$ | 320 | 180 | 700 | 4 | 750 |

TABLE 1: The core mechanical and electrical parameters of the two MSS used for the data recording.

| | beam width | range | | mechanical | max. field |
|------------|---------------------------|---------|---------|---|---------------|
| | $H \times V$ [deg] | min [m] | max [m] | steps [deg] | of view [deg] |
| Ping360 | $2^\circ \times 25^\circ$ | 0.75 | 50 | $0.9^\circ, 1.8^\circ, 3.6^\circ$ | 360° |
| Micron DST | $3^\circ \times 35^\circ$ | 0.3 | 75 | $0.45^\circ, 0.9^\circ, 1.8^\circ, 3.6^\circ$ | 360° |

TABLE 2: The basic sensor parameters of the two MSS.

As GNSS information is not available underwater, the localization, respectively relative motion estimation must be based on navigation sensors [25]–[27], i.e., typically a DVL and an IMU. In our Bremen datasets, recordings from a Waterlinked A50 in the high-performance version [28] and an Xsens MTi-300 IMU [29] are provided.

The transducer of the A50 DVL operates at 1MHz. It has a 0.05 – 50m altitude range, a 4 – 15Hz ping rate depending on the altitude, and a nominal velocity resolution of 0.1mm/s at $\pm 0.1\%$ accuracy for the performance version. It is marketed as the default DVL for the BlueROV2, among others due to its small size of 66mm diameter and 25mm height as well as the low average power consumption of 4W. The A50 version used in the trials has a depth rating of 300m. The Xsens MTi-300 IMU is based on Micro-Electro-Mechanical-Systems (MEMS) for the 6-axis gyroscope and acceleration measurements combined with a magnetometer. It achieves a good accuracy, especially within the class of MEMS-devices, due to very good ex-factory calibration. It has a nominal accuracy of 0.2° root mean squared error (RMS) for roll and pitch, and 1° RMS for yaw. The bias within a run is $10^\circ/h$ and the update rate is 200Hz.

As a fringe benefit, our datasets can be used for research on underwater navigation [25]–[27] based on the according sensors, i.e., the IMU and the DVL, by comparing the estimated localization with the ground truth without taking any of the sonar data into account. To further support this, we also included additional data in some of the datasets, namely PixHawk PX4 IMU data and recordings of motor data. The very basic IMU in the PixHawk PX4 flight-controller fuses data from two 6-axis MEMS-chips, namely a ICM-20689 and a BMI055, plus a IST8310 magnetometer. It can serve as a comparison basis to the also MEMS-based but higher-quality Xsens MTi-300. The motor data can be used to study hydrodynamical models for navigation.

C. THE ENVIRONMENT AND THE MOTION CAPTURE SYSTEM

The trials are carried out in the test basin at Robotics Innovation Center (RIC) of the German Research Center for Artificial Intelligence (DFKI GmbH) in Bremen, Germany. The test basin (Fig. 2) is quite large and deep with $23m \times 19m \times 8m$, containing 3.4 million liters of saltwater. In addition, it is equipped with optical motion capture system (MCS) from

Qualisys that can accurately track the pose of multiple objects with respect to the basin, thereby providing highly accurate ground truth data. A total of 12 cameras with 12 megapixels each detect highly reflecting markers attached to the robot to estimate its pose. The spherical markers used to track the BlueROV2 are shown in Fig. 1. The calibration of the system includes the estimation of the rigid transformations between the markers that are placed on the robot as well as of the cameras themselves.

The system provides an accuracy of about 4mm, i.e., much better than state-of-the-art RTK GPS, at a very high update rate of 300Hz. Furthermore, the MCS provides in contrast to GNSS also orientation measurement. Hence, the full pose information is available as ground truth.

III. OVERVIEW OF THE DATASETS

The data records consist of 14 datasets. There are 13 main datasets with ground truth. A 14th dataset is provided where the robot is kept in a fixed position without ground truth localization. This 14th dataset can be used for calibrating or analyzing the odometry sensors, i.e., the two IMUs and the DVL, if this is of interest for the method(s) that are investigated with the data. Furthermore, the sensor locations on the robot are provided as part of the datasets and their documentation (Fig.3).

The datasets are stored as ROS2-bags, respectively YAML-files - see also section "Usage Notes". They are available for download via IEEE Dataport (<https://doi.org/10.21227/dy87-1k42>) as a single zip-file. Furthermore, a documentation-paper with technical information on the data and its usage is provided under the above DOI on IEEE Dataport.

The parameter settings and the trial complexity for each dataset are shown in Tab.3. The datasets 1-8 cover typical state-of-the-art scenarios. The environment is static and there are no aspects that introduce some added complexity. The datasets are based on different parameter settings for the MSS, namely with respect to range and stepping angle, as well as the speed of the robot.

The changes in speed are of interest as a higher velocity of the UUV makes navigation more challenging. A rough indication in form of *fast* (*f*) or *slow* (*s*) velocity is hence provided for each dataset in Tab. 3. For a precise determination of the UUV's velocity, the ground truth data can and should be used.

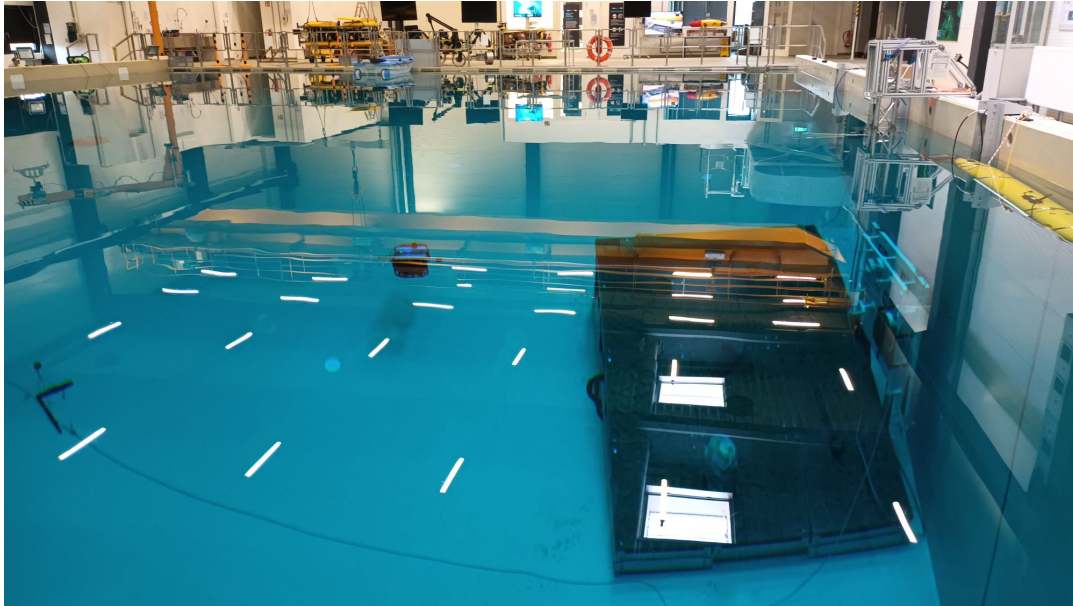


FIGURE 2: A snapshot of the DFKI test tank where the data was recorded. The 12 Qualisys cameras for motion tracking are roughly placed in regular distances - a CAD layout of the pool and the exact locations of the cameras are provided together with the data-sets.

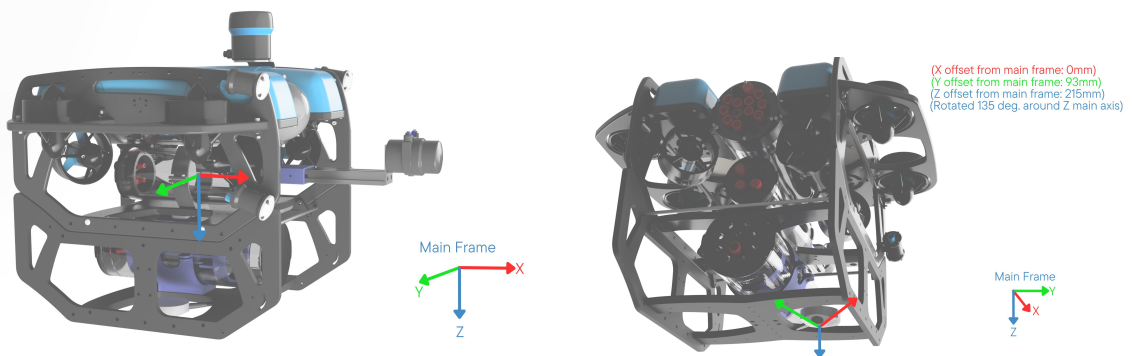


FIGURE 3: A BlueROV2 CAD model is used to provide the locations of all sensors as part of the datasets and their documentation. The reference frame of the robot itself is placed at the geometrical center of the robot (left). The locations of the sensor frames, e.g., for the DVL (right), are provided relative to the robot frame.

The range and the stepping angle of the MSS as well as the UUV's velocity influence the input to the registration methods that may be used for mapping, especially in the context of SLAM. Higher velocity and shorter range lead to less overlap between consecutive scans that are to be registered. Higher stepping angles lead to lower resolution. Furthermore, there is the aspect of motion compensation, i.e., due to the design principles of MSS, multiple scan-lines have to be integrated to form scans that are to be registered. Hence, pose-estimations using short time navigation windows are needed in this scan-formation. The difficulty to do a successful scan-formation is therefore also influenced by these parameters, especially by the velocity of the UUV.

The three datasets 9-11 feature the combined use of two MSS, namely the Ping360 and the Micron DST. The main

purpose of the additional MSS is to generate a scenario with acoustic "pollution", i.e., non-trivial noise as both sonars operate in distinct but neighboring frequency ranges (Tab. 1). While the Ping360 still provides reasonable range data, the quality is clearly worse than in the datasets 1-8. The data is hence of interest to test the robustness of, e.g., range extraction, registration, and SLAM methods. Furthermore, the data of the Micron DST, which is less affected by the dual operation due to its chirp processing, can be used to study the navigation in combination with (simple) bathymetry or 3D mapping.

The datasets 12 and 13 include dynamics in the scene, which is an underrepresented topic in the context of research on the use of MSS. The dynamics are generated with a large Autonomous Underwater Vehicle (AUV), which moves in the

| data-set | #scan-lines | Ping360 | | Micron | | DVL A50 | IMU | | | mot. val. | dyn. sce. | vel. f/s |
|----------|-------------|-----------|------------|-----------|------------|---------|-----|-----|---|-----------|-----------|----------|
| | | range [m] | step [deg] | range [m] | step [deg] | | MTi | PX4 | | | | |
| 1 | 6,993 | 15 | 0.9° | — | — | • | • | - | - | - | - | s |
| 2 | 7,361 | 15 | 0.9° | — | — | • | • | • | - | - | - | f |
| 3 | 9,198 | 15 | 3.6° | — | — | • | • | • | - | - | - | s |
| 4 | 6,608 | 15 | 3.6° | — | — | • | • | • | - | - | - | f |
| 5 | 14,578 | 7 | 0.9° | — | — | • | • | • | - | - | - | s |
| 6 | 7,784 | 7 | 0.9° | — | — | • | • | • | - | - | - | f |
| 7 | 9,146 | 7 | 3.6° | — | — | • | • | • | - | - | - | s |
| 8 | 7,074 | 7 | 3.6° | — | — | • | • | • | - | - | - | f |
| 9 | 12,396 | 15 | 0.9° | 15 | 0.9° | • | • | • | • | - | - | s |
| 10 | 7,400 | 7 | 0.9° | 15 | 0.9° | • | • | • | • | - | - | s |
| 11 | 13,346 | 20 | 0.9° | 20 | 0.9° | • | • | • | • | - | - | s |
| 12 | 7,339 | 15 | 1.8° | — | — | • | • | • | • | • | • | s |
| 13 | 7,645 | 7 | 1.8° | — | — | • | • | • | • | • | • | s |

TABLE 3: The settings and properties for each dataset, i.e., the total number of scanlines, settings for the range and the stepping angle (step) of the respective MSS, inclusion of the different navigation data from the A50 DVL, the Xsens MTi-300 IMU (MTi), the PixHawk PX4 IMU (PX4), and the motor values (mot.val.), as well as the presence of dynamics in the scene (dyn.sce.). The UUV is operated with either fast (f) or slow (s) velocity (vel.). In the fast version, the robot additionally randomly rotates around its own z-axis.

field of view of the Ping360. As usual with dynamics, this generates challenges for the registration of scans, e.g., in the context of mapping and SLAM.

IV. TECHNICAL VALIDATION

The ground truth of the robot poses plus the known geometry of the pool including the rigid camera poses allow a large range of quantitative analyzes depending on the application case. Suited metrics can be path-based, e.g., the mean-squared-error (MSE) and the variance of the estimated and the real pose, i.e., in $(x, y, \theta)^T$, or the drift, i.e., the Euclidean distance between the estimated and the ground truth position in (x, y) . There are also the various map-based metrics that can be used.

For a technical validation of the datasets, we first provide ground truth based visualizations of the datasets in the following section. They illustrate the advantage of accurate full pose information, i.e., the scan-lines can be rendered into accurate maps - within the limits of the raw MSS data - based on just the optical tracking. These maps also provide an overview of the data that supplements the information provided in Tab. 3.

Second, a baseline method for using the sensor data is provided. It is based on standard navigation with dead reckoning, i.e., an Extended Kalman Filter (EKF) is used to compute localization estimates based on the IMU and DVL data. The related pose-estimates are then used to render the scan-lines into maps and to provide a quantitative analysis of this baseline solution.

A. VISUALIZATIONS BASED ON GROUND TRUTH

The 13 datasets are visualized with the data from the Ping360 and the ground truth localization; the according maps are shown in Figures. 4-6. For each scan-line s_i of the MSS, the ground truth pose ${}^{GT}p_i = {}^{GT}(x_i, y_i, \theta_i)^T$ of the UUV is used to render s_i into the map. More precisely, the known fixed frame ${}^{MSS}\mathcal{F}$ of the MSS relative to the vehicle frame ${}^{UUV}\mathcal{F}$ is used to determine the absolute position and orientation

of the start of the sonar-beam to integrate the amplitudes of returns along the beam into the map. The exact frames of all sensors relative to the vehicle's center and hence to the ground-truth are provided in the technical documentation that complements this article.

On the left of each map, a rainbow color-palette for the normalized amplitude of the returns of the MSS is shown. The walls of the pool generate a clearly distinguishable back-scatter in the range of ca. 0.35 to 0.6; it is occasionally even higher up to the maximum, e.g., if the sonar-beam is perpendicularly facing a wall. The open water as well as ranges beyond the wall are also clearly perceivable with very low amplitudes near 0, i.e., they are just background noise. Values of exactly 0 indicate that these parts have not been covered by any sensor beam. The ground-truth path of the UUV is also shown in each visualization of the datasets. On the right of each map, a heat color-palette provides information on the number of cameras that can track the robot during its motion. Due to self-occlusion, not all cameras can always detect sufficiently many markers on the robot. The maximum is 10 out of 12 cameras. Typically, 7 to 8 cameras detect it. In some parts of the trajectory, this can be lower, but the position and especially orientation accuracy is still very high. More details are provided in the datasets themselves. Furthermore, the ground truth locations of the cameras are shown in each map. They are marked with red crosses.

Fig. 4 shows the visualizations of the datasets 1-8. Especially the influence of the range parameter can be seen. The whole pool is not covered with the shorter range setting of the MSS in the datasets 5-8. Accordingly, the underlying scans also have much more limited views of the pool, which makes registration more challenging than in the datasets 1-4.

The three datasets 9-11 are visualized in Fig. 5, where the Micron DST is used to generate acoustic disturbances for the Ping360. This is reflected in a higher noise level in the sonar-beams. The representation of the walls of the pools becomes less pronounced. This data is hence of particular interest to

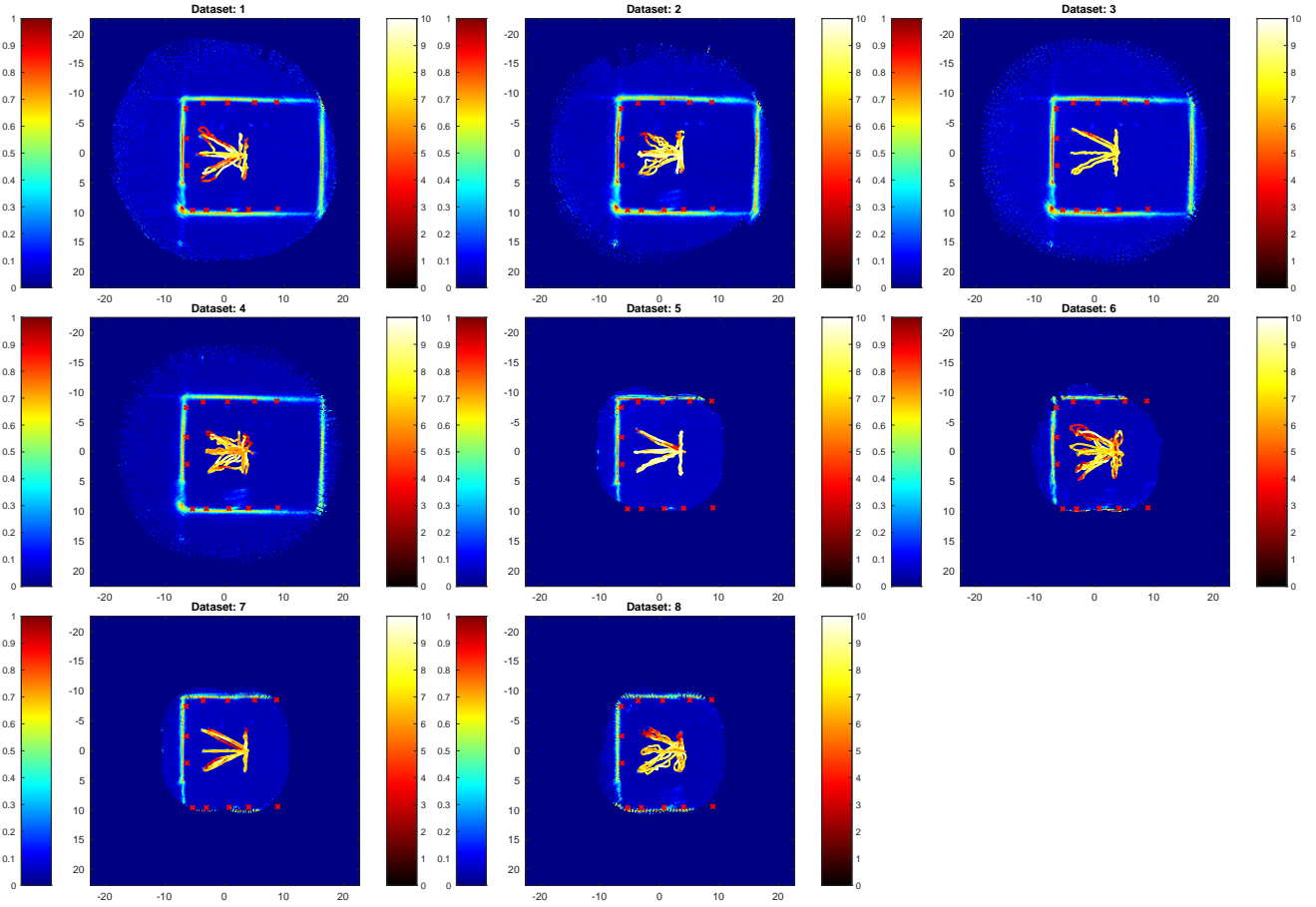


FIGURE 4: Visualizations of the datasets 1 to 8 with a static environment and different parameter settings for range and stepping angle of the Ping360 plus different speeds of the UUV. For a detailed description, please refer to the text.

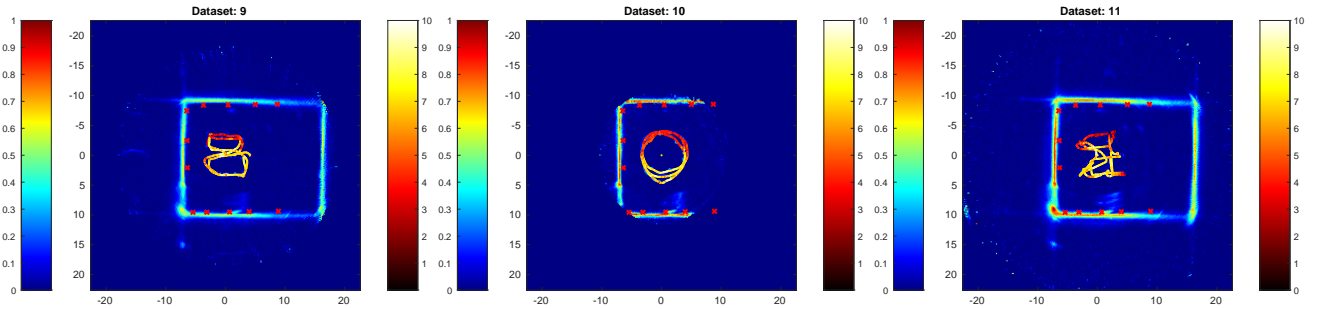


FIGURE 5: Visualizations of the datasets 9 to 11 where a second MSS in form of a Micron DST generates acoustic disturbances.

test the robustness of range extraction methods as well as of registration methods.

The visualizations of the two datasets 12 and 13 are shown in Fig. 6. In these, an AUV generates dynamics in the scene. On the right of Fig. 6, a zoom into the map of dataset 12 shows the area where the AUV is moving. The multiple locations where the AUV was sensed are only faintly represented in the maps as the according data is accumulated in the occupancy grid, i.e., multiple views of empty space are fused with a few views of an obstacle at the times when the AUV passed there. The effects of the 2nd vehicle are accordingly more

pronounced in individual scans, where they constitute substantial dynamic effects between consecutive scans that are to be registered. Furthermore, the AUV generates occlusions and scattering, which is for example visible in Fig. 6 in dataset 12: the representation of the wall at the right-hand side of the pool is, e.g., affected by this.

B. AN EXTENDED KALMAN FILTER (EKF) AS BASELINE METHOD

To ease the evaluation of third-party methods and approaches, a baseline solution for navigation and mapping is provided.

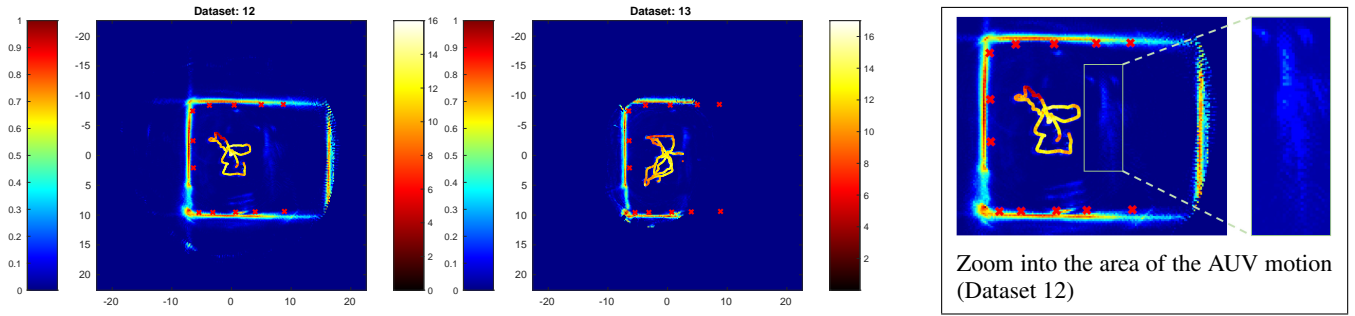


FIGURE 6: Visualizations of the datasets 12 and 13 where an AUV in the field of view of the sonar generates dynamics in the scene. On the right, a zoom into the area where the AUV is moving is shown for dataset 12.

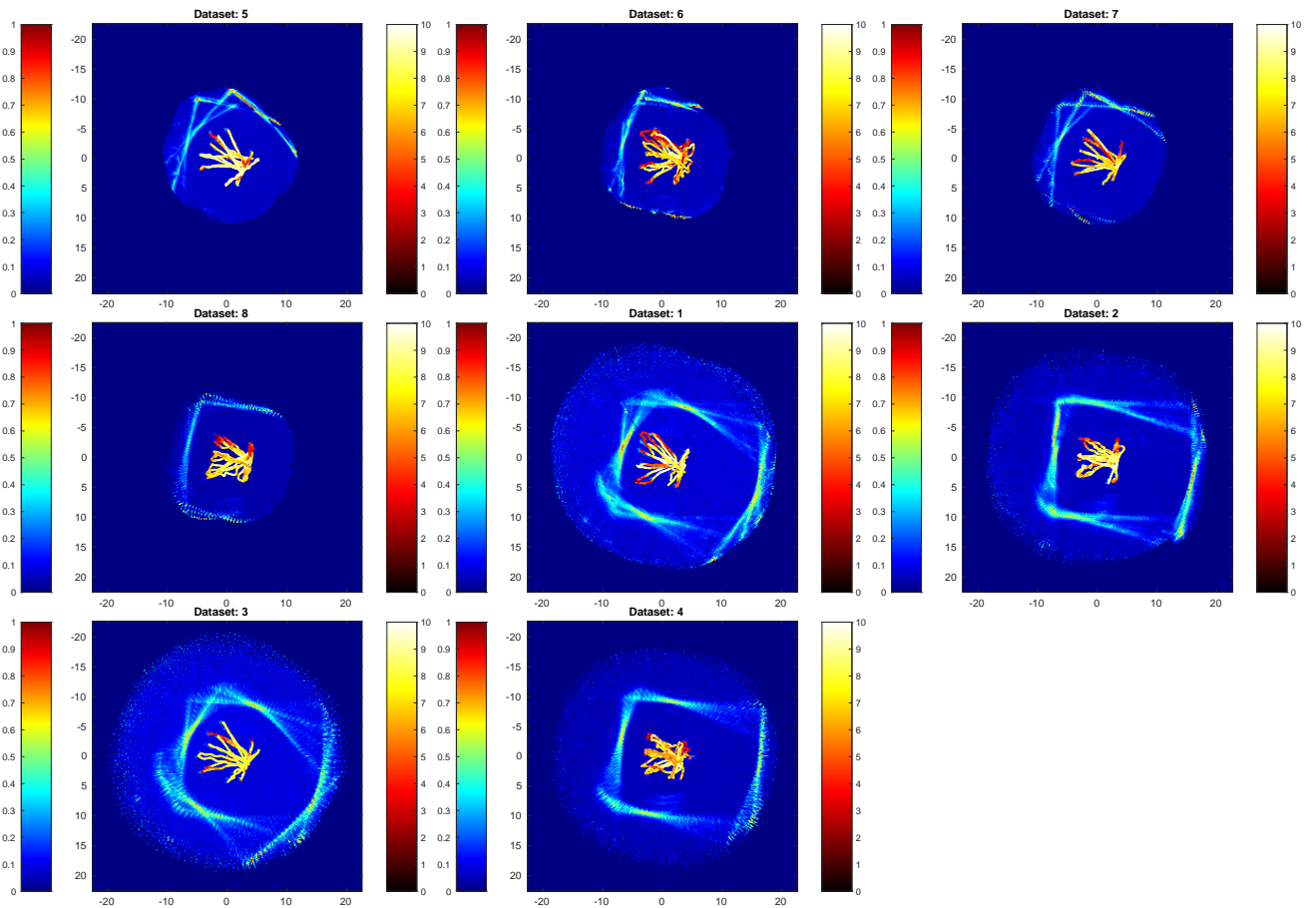


FIGURE 7: Maps with EKF-navigation using the datasets 1 to 8 with a static environment.

It is based on the standard method for core navigation using an Extended Kalman Filter (EKF) operating on the DVL and IMU data. The EKF provides motion estimation and path integration, i.e., pose-estimates ${}^{EKF}\hat{p}_t = {}^{EKF}\hat{p}_t(x_t, y_t, \theta_t)^T$ of the UUV. Like for the ground truth visualizations, the pose ${}^{EKF}\hat{p}_t$ is used to render the corresponding scan-line of the Ping360 into an occupancy map. The code of the baseline solution with the plain vanilla implementation of the EKF is provided as described below in sections "Usage Notes" and "Code Availability".

The Fig. 7-9 show the maps generated with the datasets.

The data is again partitioned according to a static environment and different parameter settings (Fig. 7, datasets 1-8), the presence of an additional MSS and hence of acoustic disturbances (Fig. 8, datasets 9-11), and dynamics scenes (Fig. 9, datasets 12&13).

As can be expected, the simple baseline solution with EKF-based navigation is quite imprecise as can be directly seen in the visualized maps. Path-integration has an element of a random walk. Especially if a large angular error in the pose-estimation happens by coincidence or due to a form of bump-noise, this has strong lasting effects on the consecutive

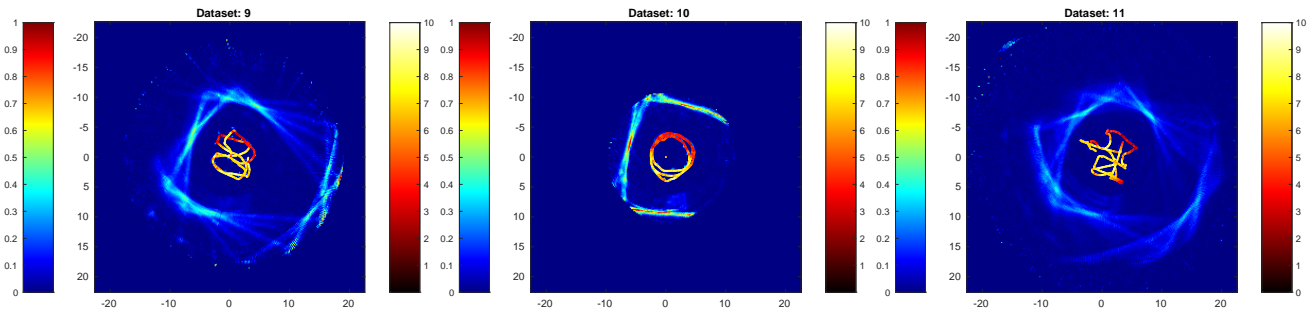


FIGURE 8: Maps with EKF-navigation using the datasets 9 to 11 with a 2nd MSS, i.e., with acoustic disturbances.

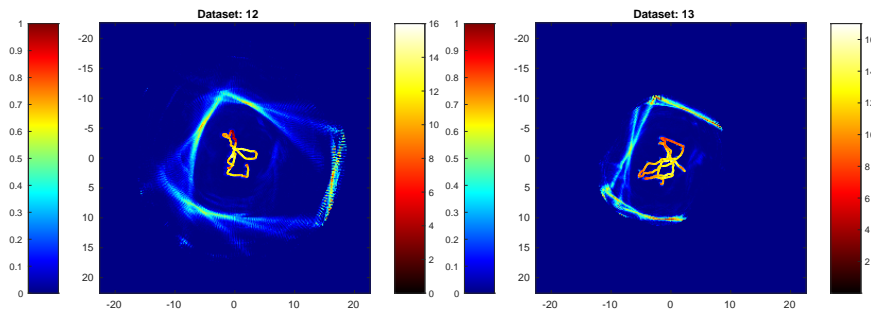


FIGURE 9: Maps with EKF-navigation using the datasets 12 and 13 with a 2nd UUV, i.e., with dynamics in the scene.

| data-set | EKF performance | | | drift $\ \cdot\ _2$ (m) |
|----------|------------------------------|------------------------------|-------------------------------------|----------------------------|
| | pose MSE | | | |
| | $\Delta x : \mu, \sigma$ (m) | $\Delta y : \mu, \sigma$ (m) | $\Delta \theta : \mu, \sigma$ (rad) | |
| 1 | 0.73 ± 0.56 | 0.57 ± 0.55 | 0.33 ± 0.2 | 2.0 |
| 2 | 0.52 ± 0.51 | 0.23 ± 0.19 | 0.13 ± 0.14 | 1.64 |
| 3 | 0.89 ± 0.78 | 0.72 ± 0.76 | 0.45 ± 0.26 | 2.53 |
| 4 | 0.36 ± 0.28 | 0.35 ± 0.34 | 0.19 ± 0.2 | 1.37 |
| 5 | 1.06 ± 0.92 | 0.77 ± 0.78 | 0.54 ± 0.31 | 2.99 |
| 6 | 0.47 ± 0.44 | 0.38 ± 0.31 | 0.21 ± 0.14 | 1.32 |
| 7 | 0.84 ± 0.67 | 0.57 ± 0.55 | 0.42 ± 0.24 | 2.46 |
| 8 | 0.56 ± 0.35 | 0.33 ± 0.27 | 0.2 ± 0.1 | 1.62 |
| 9 | 0.74 ± 0.61 | 0.78 ± 0.67 | 0.44 ± 0.30 | 3.13 |
| 10 | 0.58 ± 0.36 | 0.57 ± 0.52 | 0.21 ± 0.13 | 1.3 |
| 11 | 1.36 ± 1.39 | 1.06 ± 1.12 | 0.67 ± 0.43 | 2.28 |
| 12 | 0.36 ± 0.33 | 0.78 ± 0.66 | 0.36 ± 0.23 | 1.93 |
| 13 | 0.76 ± 0.66 | 0.48 ± 0.47 | 0.39 ± 0.23 | 2.47 |

TABLE 4: The results of two example error metrics for a quantitative analysis of the baseline solution with an EKF, namely the mean μ and the variance σ of a pose-based mean squared error (MSE) and the total drift, i.e., the Euclidean Distance $\|\cdot\|_2$ between the final estimated and the real position of the UUV.

pose-estimates. When or how often this form of error occurs over the duration of a trajectory is mainly a matter of chance and independent of parameter settings of the MSS or the conditions in the environment. This is of course different if more sophisticated methods are evaluated with the datasets as described above in section "Data Records", i.e., if the registration of scans or SLAM are used.

For the sake of completeness, two quantitative analyzes of the results of the baseline solution are provided in Tab. 4. The mean-squared-error (MSE) of the pose and the total drift are used as two different metrics for evaluating the results. More

precisely, the mean μ and the variance σ of the MSE of the differences $\Delta x, \Delta y, \Delta \theta$ in the 3 degrees-of-freedom (dof) of the estimated poses ${}^{EKF}p_t$ and the ground truth poses ${}^{GT}p_t$ is provided. Furthermore, the total drift, i.e., the Euclidean distance $\|({}^{EKF}x_N, {}^{EKF}y_N), ({}^{GT}x_N, {}^{GT}y_N)\|_2$ between the estimated final location $({}^{EKF}x_N, {}^{EKF}y_N)$ and the ground truth location $({}^{GT}x_N, {}^{GT}y_N)$ at the end of each trajectory is given.

V. USAGE NOTES

As mentioned above, access to the data and additional material like links to the related code and a technical documentation as white-paper is provided via IEEE Dataport (<https://doi.org/10.21227/dy87-1k42>). The message definitions of the ROS2 bags are available as code on Github that can be directly used and in addition, they are described in the accompanying technical white-paper on IEEE Dataport. The white-paper also provides information on the location of each sensor frame relative to the reference-frame of the UUV itself.

All code that is directly related to the datasets and its description in this article is freely available under a *Creative Commons Attribution-NonCommercial (CC BY-NC)*¹ license². The Robot Operating System (ROS) that is used to operate the UUV and to record the data in ROS2 bags is freely available under the standard three-clause BSD license. The additional copies of the data in YAML-files can be read and processed with a wide range of free software packages for data science and mathematical processing, e.g., according Python libraries.

¹<https://creativecommons.org/licenses/by-nc/4.0/>

²Please note that the use of the data is restricted while there is no related academic paper published, yet.

VI. CONCLUSIONS

Collections of data from Mechanical Scanning Sonars (MSS) were presented, i.e., data from popular underwater sensors for Unmanned Underwater Vehicles (UUV) due to their low cost, small size, and low power consumption. The core contribution is the provision of precise ground truth data for the full pose, i.e., the localization with position and orientation, of the UUV in addition to standard navigation sensors, i.e., an Inertial Measurement Unit (IMU) and a Doppler Velocity Log (DVL). More precisely, the UUV is globally localized with a high precision optical tracking system in a large research pool. Furthermore, different parameter settings and environment conditions are covered, and baseline solutions for localization and mapping are provided. This is of interest for multiple research areas related to MSS, e.g., extraction of range information, registration of sonar scans, and especially mapping including Simultaneous Localization and Mapping (SLAM).

REFERENCES

- [1] N. O. (NOAA) and A. Administration, "Bathymetric data viewer," 2024. [Online]. Available: <https://www.ncei.noaa.gov/maps/bathymetry/>
- [2] D. Potap, A. Jaszcz, N. Wawrzyniak, and G. Zaniewicz, "Bilinear pooling with poisoning detection module for automatic side scan sonar data analysis," *IEEE Access*, vol. 11, pp. 72 477–72 484, 2023.
- [3] T. Yulin, S. Jin, G. Bian, and Y. Zhang, "Shipwreck target recognition in side-scan sonar images by improved yolov3 model based on transfer learning," *IEEE Access*, vol. 8, pp. 173 450–173 460, 2020.
- [4] K. Xie, J. Yang, and K. Qiu, "A dataset with multibeam forward-looking sonar for underwater object detection," *Scientific Data*, vol. 9, no. 1, p. 739, 2022. [Online]. Available: <https://doi.org/10.1038/s41597-022-01854-w>
- [5] X. Qin, X. Luo, Z. Wu, and J. Shang, "Optimizing the sediment classification of small side-scan sonar images based on deep learning," *IEEE Access*, vol. 9, pp. 29 416–29 428, 2021.
- [6] L. Jin, H. Liang, and C. Yang, "Accurate underwater atr in forward-looking sonar imagery using deep convolutional neural networks," *IEEE Access*, vol. 7, pp. 125 522–125 531, 2019.
- [7] X. Luo, X. Qin, Z. Wu, F. Yang, M. Wang, and J. Shang, "Sediment classification of small-size seabed acoustic images using convolutional neural networks," *IEEE Access*, vol. 7, pp. 98 331–98 339, 2019.
- [8] R. P. Gorman and T. J. Sejnowski, "Analysis of hidden units in a layered network trained to classify sonar targets," *Neural Networks*, vol. 1, no. 1, pp. 75–89, 1988. [Online]. Available: <https://www.sciencedirect.com/science/article/pii/0893608088900238>
- [9] T. Hansen and A. Birk, "Synthetic scan formation for underwater mapping with low-cost mechanical scanning sonars (mss)," *IEEE Access*, vol. 11, pp. 96,854–96,864, 2023, open Access.
- [10] T. Hansen, F. Buda, and A. Birk, "Underwater exploration with sonar of the flooded basement of a ww-ii submarine bunker in the context of digitization of cultural heritage," in *MTS/IEEE OCEANS*, 2023, Conference Proceedings, pp. 1–5.
- [11] Z. Xu, H. Qiu, M. Dong, H. Wang, and C. Wang, "Underwater simultaneous localization and mapping based on 2d-slam framework," in *IEEE International Conference on Unmanned Systems (ICUS)*, 2022, Conference Proceedings, pp. 184–189.
- [12] L. Chen, A. Yang, H. Hu, and W. Naem, "Rbpf-msis: Toward rao-blackwellized particle filter slam for autonomous underwater vehicle with slow mechanical scanning imaging sonar," *IEEE Systems Journal*, vol. 14, no. 3, pp. 3301–3312, 2020.
- [13] M. Jiang, S. Song, J. M. Herrmann, J. H. Li, Y. Li, Z. Hu, Z. Li, J. Liu, S. Li, and X. Feng, "Underwater loop-closure detection for mechanical scanning imaging sonar by filtering the similarity matrix with probability hypothesis density filter," *IEEE Access*, vol. 7, pp. 166 614–166 628, 2019.
- [14] M. Jiang, S. Song, F. Tang, Y. Li, J. Liu, and X. Feng, "Scan registration for underwater mechanical scanning imaging sonar using symmetrical kullback-leibler divergence," *Journal of Electronic Imaging*, vol. 28, no. 1, 2019.
- [15] A. Mallios, P. Ridaio, D. Ribas, and E. Hernández, "Scan matching slam in underwater environments," *Autonomous Robots*, vol. 36, no. 3, pp. 181–198, 2014. [Online]. Available: <https://doi.org/10.1007/s10514-013-9345-0>
- [16] A. Burguera, Y. González, and G. Oliver, "Underwater slam with robocentric trajectory using a mechanically scanned imaging sonar," in *IEEE/RSJ International Conference on Intelligent Robots and Systems*, 2011, Conference Proceedings, pp. 3577–3582.
- [17] A. Mallios, P. Ridaio, M. Carreras, and E. Hernandez, "Navigating and mapping with the sparus auv in a natural and unstructured underwater environment," in *OCEANS 2011*, 2011, Conference Proceedings, pp. 1–7.
- [18] H. Bülow, M. Pflugstorn, and A. Birk, "Using robust spectral registration for scan matching of sonar range data," in *7th Symposium on Intelligent Autonomous Vehicles (IAV), IFAC*, IFAC, 2010, Conference Proceedings.
- [19] A. Burguera, G. Oliver, and Y. González, "Scan-based slam with trajectory correction in underwater environments," in *IEEE/RSJ International Conference on Intelligent Robots and Systems*, 2010, Conference Proceedings, pp. 2546–2551.
- [20] A. Mallios, P. Ridaio, E. Hernandez, D. Ribas, F. Maurelli, and Y. Petillot, "Pose-based slam with probabilistic scan matching algorithm using a mechanical scanned imaging sonar," in *OCEANS 2009*, 2009, Conference Proceedings, pp. 1–6. [Online]. Available: 10.1109/OCEANSE.2009.5278219
- [21] E. Hernandez, P. Ridaio, D. Ribas, and A. Mallios, "Probabilistic sonar scan matching for an auv," in *Intelligent Robots and Systems, 2009. IROS 2009. IEEE/RSJ International Conference on*, 2009, Conference Proceedings, pp. 255–260. [Online]. Available: 10.1109/IROS.2009.5354656
- [22] D. Ribas, P. Ridaio, J. D. Tardos, and J. Neira, "Underwater slam in man-made structured environments," *Journal of Field Robotics*, vol. 25, no. 11/12, pp. 898–921, 2008.
- [23] D. Ribas, P. Ridaio, J. Domingo Tardos, and J. Neira, "Underwater slam in a marina environment," in *Intelligent Robots and Systems, 2007. IROS 2007. IEEE/RSJ International Conference on*, P. Ridaio, Ed., 2007, Conference Proceedings, pp. 1455–1460.
- [24] BlueRobotics, "Bluerov2," 2023. [Online]. Available: <https://bluerobotics.com/store/rov/bluerov2/>
- [25] F. Maurelli, S. Krupinski, X. Xiang, and Y. Petillot, "Auv localisation: a review of passive and active techniques," *International Journal of Intelligent Robotics and Applications*, vol. 6, no. 2, pp. 246–269, 2022. [Online]. Available: <https://doi.org/10.1007/s41315-021-00215-x>
- [26] L. Paull, M. Seto, S. Saeedi, and J. J. Leonard, "Navigation for underwater vehicles," in *Encyclopedia of Robotics*, M. H. Ang, O. Khatib, and B. Siciliano, Eds. Berlin, Heidelberg: Springer, 2018, pp. 1–15. [Online]. Available: https://doi.org/10.1007/978-3-642-41610-1_15-1
- [27] L. Paull, S. Saeedi, M. Seto, and H. Li, "Auv navigation and localization: A review," *IEEE Journal of Oceanic Engineering*, vol. 39, no. 1, pp. 131–149, 2014.
- [28] WaterLinked, "A50 dvl," 2023. [Online]. Available: <https://waterlinked.com/dvl-a50>
- [29] Xsense, "Mti-300 hrs," 2023. [Online]. Available: <https://www.movella.com/products/sensor-modules/xsens-mti-300-hrs>



TIM HANSEN received the B.S. and M.S. degree in mechatronics engineering from the Technical University Hamburg, Germany in 2020. Since 2021 PhD student at Constructor University Bremen, Germany. Already before the M.S. degree, the focus lied in micro underwater robotics, with the focus on state estimation. In his current research the focus lies in underwater robotic systems, that are able to observe the environment, while still being low-cost.



BOGDAN BELENIS received his BSc in Robotics and Intelligent Systems (RIS) from Constructor University in June 2023. He is among others active as a marine robotics researcher at Constructor University, e.g., providing mechatronics developments and the migration of underwater robot code from ROS to ROS2.



MIGUEL BANDE FIRVIDA received a Dipl. in Aerospace Engineering from the Universitat Politècnica de Catalunya, Spain in 2013 and a M.Sc. in Systems Engineering from the University of Bremen, Germany, in 2018. Since 2019, he has been working as a researcher at the German Research Center for Artificial Intelligence (DFKI) as part of the Maritime Robotics team. His current research focuses on applying modern machine learning methods for underwater robotic percep-

tion with optical, acoustic and magnetic modalities. Previously, he worked at Bremen Institute for Production and Logistics (BIBA), Germany, also as researcher, where he investigated decentralized systems and co-developed the celloveyor, a modular conveyor technology for flexible material flow.



TOM CREUTZ received his B.Sc. degree in Computer Science at Technische Universität Dresden before moving to Bremen to obtain his M.Sc. in Computer Science at Universität Bremen. Since end of 2021 he is working at Deutsches Forschungszentrum für Künstliche Intelligenz (DFKI) in Bremen as a researcher in the maritime robotics team. He is mostly working on localization, autonomous behavior, mission planning and software engineering problems.



ANDREAS BIRK (M'97) received his PhD (Dr. rer.nat) in 1995 from the Universität des Saarlandes, Saarbrücken, Germany where he previously studied Computer Science from fall 1989 to spring 1993 for his MSc and BSc degree (Diplom). He is since 2011 a full professor in Electrical Engineering and Computer Science at Constructor University Bremen, Germany, where he started in 2001 as associate professor. Before, he worked from 1996 to 2001 as a postdoc in the AI-lab of the

Vrije Universiteit Brussel (VUB), Brussels, Belgium, where he was among others from 1998 to 2001 a Research Fellow of the Flemish Society of Applied Research (IWT).

...